Atmospheric Research 193 (2017) 73–82

Contents lists available at ScienceDirect

Atmospheric Research

journal homepage: www.elsevier.com/locate/atmosres

Drought sensitivity mapping using two one-class support vector machine algorithms

Majid Shadman Roodposhti[a,*], Taher Safarrad[b], Himan Shahabi[c]

[a] Discipline of Geography and Spatial Sciences, School of Land & Food, University of Tasmania, Australia
[b] Department of Geography and Urban Planning Faculty of Humanities and Social Science, University of Mazandaran, Babolsar, Iran
[c] Department of Geomorphology, Faculty of Natural Resources, University of Kurdistan, Sanandaj, Iran

ARTICLE INFO

Keywords:
Drought sensitivity map (DSM)
Enhanced vegetation index (EVI)
Standardised precipitation index (SPI)
One-class support vector machine (OC-SVM)
Kermanshah

ABSTRACT

This paper investigates the use of standardised precipitation index (SPI) and the enhanced vegetation index (EVI) as indicators of soil moisture. On the other hand, we attempted to produce a drought sensitivity map (DSM) for vegetation cover using two one-class support vector machine (OC-SVM) algorithms. In order to achieve promising results a combination of both 30 years statistical data (1978 to 2008) of synoptic stations and 10 years MODIS imagery archive (2001 to 2010) are used within the boundary of Kermanshah province, Iran. The synoptic data and MODIS imagery were used for extraction of SPI and EVI, respectively. The objective is, therefore, to explore meaningful changes of vegetation in response to drought anomalies, in the first step, and further extraction of reliable spatio-temporal patterns of drought sensitivity using efficient classification technique and spatial criteria, in the next step. To this end, four main criteria including elevation, slope, aspect and geomorphic classes are considered for DSM using two OC-SVM algorithms. Results of the analysis showed distinct spatio-temporal patterns of drought impacts on vegetation cover. The receiver operating characteristics (ROC) curves for the proposed DSM was used along with the simple overlay technique for accuracy assessment phase and the area under curve (AUC = 0.80) value was calculated.

1. Introduction

Global warming affects evapotranspiration, which is the movement of water into the atmosphere from land, water surfaces and plants due to evaporation and transpiration. This is expected to increase to both drought severity measure and geographic expansion of dry areas. When discussing drought, one must have a proper understanding of aridity and the difference between the two. Climatologically, aridity is defined as “the degree to which a climate lacks effective, life-promoting moisture” while drought is “a period of abnormally dry weather sufficiently long enough to cause a serious hydrological imbalance” (Hayes et al., 2011). Aridity is measured by comparing long-term average precipitation and evapotranspiration. It is obviously a permanent climatic characteristic. In this regard, the arid climate indicates that average long-term evapotranspiration is greater than average long-term precipitation value. On the other hands, drought refers to the moisture balance that is mainly estimated on the annual, seasonal or monthly basis. As opposed to aridity, drought is a transient climatic idiosyncrasy (Lioubimtseva and Adams, 2004). Despite the apparent simplicity of this definition, due to its long-term development and duration, the progressive characteristics of its impacts and spatial extent, drought is the most complex natural hazard to identify, analyse, monitor and manage (Burton, 1993; Vicente-Serrano et al., 2012; Wilhite, 2012).

Nowadays, with progressive human development and subsequent climate change, drought monitoring and impact assessment program is of great importance (Zambrano et al., 2017). In order to reduce the drought vulnerability of the affected regions, it is vital to truly comprehend spatio-temporal drought patterns and their subsequent impacts. This will facilitate fulfilments of further measures focused on promoting both drought risk mitigation and preparedness. Risk mitigation simply refers to long-term measures for reducing the risk including the development of technological solutions, legislation, land-use planning, insurance, etc. (Vicente-Serrano et al., 2012). Basically, risk mitigation measures should be implemented through accurate identification of risks and promotion of the risk perception which are acquired within preparedness phase (Bird, 2009). Preparedness refers to the development of various emergency plans and warning systems aimed for efficient decision making and acting once the disaster strikes or even it is anticipated.

* Corresponding author.
E-mail address: majid.shadman@utas.edu.au (M.S. Roodposhti).

http://dx.doi.org/10.1016/j.atmosres.2017.04.017
Received 24 February 2016; Received in revised form 14 December 2016; Accepted 4 April 2017
Available online 05 April 2017

During the last decades, different types of drought indices (DIs), including climatic or satellite-derived DIs for regional to global scale drought assessment and monitoring have been developed and implemented. Climatic DIs such as percent of normal, standardised precipitation index (SPI) (Cancelliere et al., 2007; Cui et al., 2015; He et al., 2015; Sönmez et al., 2005; Zhang et al., 2009), deciles, palmer drought severity index (PDSI) (Dai, 2011; Dai et al., 2004; Li et al., 2007), crop moisture index (CMI) (Keyantash and Dracup, 2002; Quesney et al., 2000), surface water supply index (SWSI) (Shafer and Dezman, 1982; Son et al., 2012) etc. aimed to unify thousands of bits of climatological data such as rainfall, snowpack, stream flow and other water supply indicators into a comprehensible quantitative measure. A climatic DIs typically depicts how much the climate of specified geographic location in a given period has deviated from historically established normal conditions (Jairath, 2008; Mu et al., 2013; Narasimhan and Srinivasan, 2005; Pai et al., 2011; Werick et al., 1994). On the other hand, variety of satellite DIs including: normalized difference vegetation index (NDVI), vegetation condition index (VCI), temperature condition index (TCI), enhanced vegetation index (EVI) etc. also developed to quantify the drought impact on soil and/or natural vegetation cover (Bhuiyan et al., 2006; Chang et al., 2010; Huete et al., 2002; Toulios et al., 2012).

Introduction and evaluation of novel spatial methodologies for the identifying the measure of persistence and resilience of an ecosystem despite climate change constitutes a research priority of global relevance. As drought is identified one major issues of global climate variability, therefore, we present a novel approach to assess the relative sensitivity of vegetation cover, as a major constituent of any ecosystems, to drought.

Since many different DIs have been used in drought monitoring and drought sensitivity mapping studies, in an attempt to find an optimal solution and to consolidate the accuracy of obtained results, we calculated and further compared two different DIs including: 1. The standardised precipitation index (SPI) as a climatic DI and 2. Enhanced vegetation index (EVI) as satellite-derived DI. Afterwards, we made an effort to assess vegetation cover sensitivity to drought which is simply ecosystem sensitivity to short-term climate variability and regions of amplified vegetation response (Seddon et al., 2016). A novel method to identify different sensitivity classes of a drought sensitivity map (DSM) with respect to changes in elevation, slope, aspect and geomorphic criteria is implemented for this purpose. Two one-class support vector machine (OC-SVM) algorithms were beneficially used to obtain the final DSM.

The paper is organized as follows: after a description of the study area in Section 2, a detailed definition of the material and methods of the research is described in Section 3. Section 4 presents results while Section 5 belongs to a short discussion and conclusions.

2. Description of study region

Kermanshah province is located between 32°36′ to 35°15′ N latitude and 45°24′ to 48°30′ E longitude in north-western Iran and it is considered a part of the structural zone of Folded Zagros in the boundary of Arabian and Iran plate (Fig. 1). It has a climate which is heavily influenced by the proximity of the Zagros Mountains, classified as a hot dry summer with rather cold winters and there are usually rainfalls in fall and spring. Kermanshah climate is classified as typical Mediterranean climate (Csa) in Köppen-Geiger classification.

The minimum amount of precipitation occurs in June with the average of 0 mm while the maximum amount occurs in March, with an average of 76 mm. The city's altitude and exposed location relative to westerly winds makes precipitation a little bit high with a total annual precipitation average 478.7 mm. However, at the same time, it produces huge diurnal temperature swings especially in the virtually rainless summers, which remain extremely hot during the day. The annual average temperature of Kermanshah is 14.2 °C while the average monthly temperatures vary by 27.6 °C. Kermanshah also experiences snow cover for at least a couple of weeks in winter.

Arid and semi-arid regions cover almost 40% of the world's land (Aydin, 1995; Bannayan et al., 2010) and according to the climate models during the twenty-first century in the semi-arid Mediterranean, severe water loss will be caused by the climate variability (Houghton et al., 2001).Therefore, Kermanshah province of Iran could be an ideal study area for drought studies.

3. Material and methods

3.1. Data

Here, posterior to the extensive review of the relevant literature; we selected three main categories of related geospatial data. First, 30 years (from 1978 to 2008) collection of mean monthly precipitation obtained from 13 different Iranian Meteorological Organization (IMO) stations (i.e. climatological, synoptic and rain gauge stations) throughout Kermanshah province. Second, MOD 13 or enhanced vegetation index (EVI) of Terra series to effectively use as a satellite-derived DI for 10 years from 2001 to 2010. Third, 90-meter resolution digital elevation model (DEM) products of the Shuttle Radar Topography Mission (SRTM) and geomorphic unit maps of the study region used for extraction of spatio-temporal changes of drought patterns.

We also used an inventory of the most negative and positive changes in EVI value containing 842 first negative along with 842 first positive points of EVI change for both training OC-SVM algorithm and further validation of proposed DSM. It also must be noted that database of the most negative and positive changes in EVI was produced by differentiating EVI values of mild and severe drought which have accrued during the 2006 and 2008. In terms of mentioned EVI inventory, it was randomly split into a train (≈ 67%) and test (≈ 33%) samples for training the proposed DSM and subsequent validation purpose, prior and posterior map elaboration, respectively.

3.2. Methodology

The proposed methodology has three steps: in step 1, we calculated the standardised precipitation index (SPI), as one of the most widely used climatic DIs. Accordingly, in step 2, to establish the satellite-derived DI of considered study region, the EVI was used. Finally, the obtained results of the two first steps were used for subsequent analysis of spatio-temporal changes of drought impact on vegetation cover and a drought sensitivity map was then produced using two one-class support vector machine algorithms in step 3 (see Fig. 2).

3.2.1. Standardised precipitation index (SPI)

The standardised precipitation index (SPI) was proposed by (McKee et al., 1993) and if it is not the most widely used DIs (Belal et al., 2014; Jain et al., 2010; Karavitis et al., 2011), it is considered as one of most popular DIs of drought monitoring and assessment (Jiang et al., 2008; Liu et al., 2013; Mu et al., 2013; Vicente-Serrano et al., 2012). SPI is based on the probability of precipitation for any time scale. In other words, it is a simple index which is the number of standard deviations that the observed precipitation deviates from the long-term mean (i.e. 30 years), assuming a normal distribution. The SPI was designed for quantification of precipitation deficit for various time scales. These time scales reflect the impact of drought on the availability of the different water resources. Soil moisture conditions respond to precipitation anomalies on a relatively short scale. Groundwater, stream flow, and reservoir storage reflect the longer-term precipitation anomalies. Accordingly, McKee et al. (1993) originally calculated the SPI for 3, 6, 12, 24, and 48–month time scales (see Table 1).

3.2.2. Enhanced vegetation index (EVI)

The enhanced vegetation index (EVI) is one of the most popular satellite-based vegetation indices produced for the Terra and Aqua

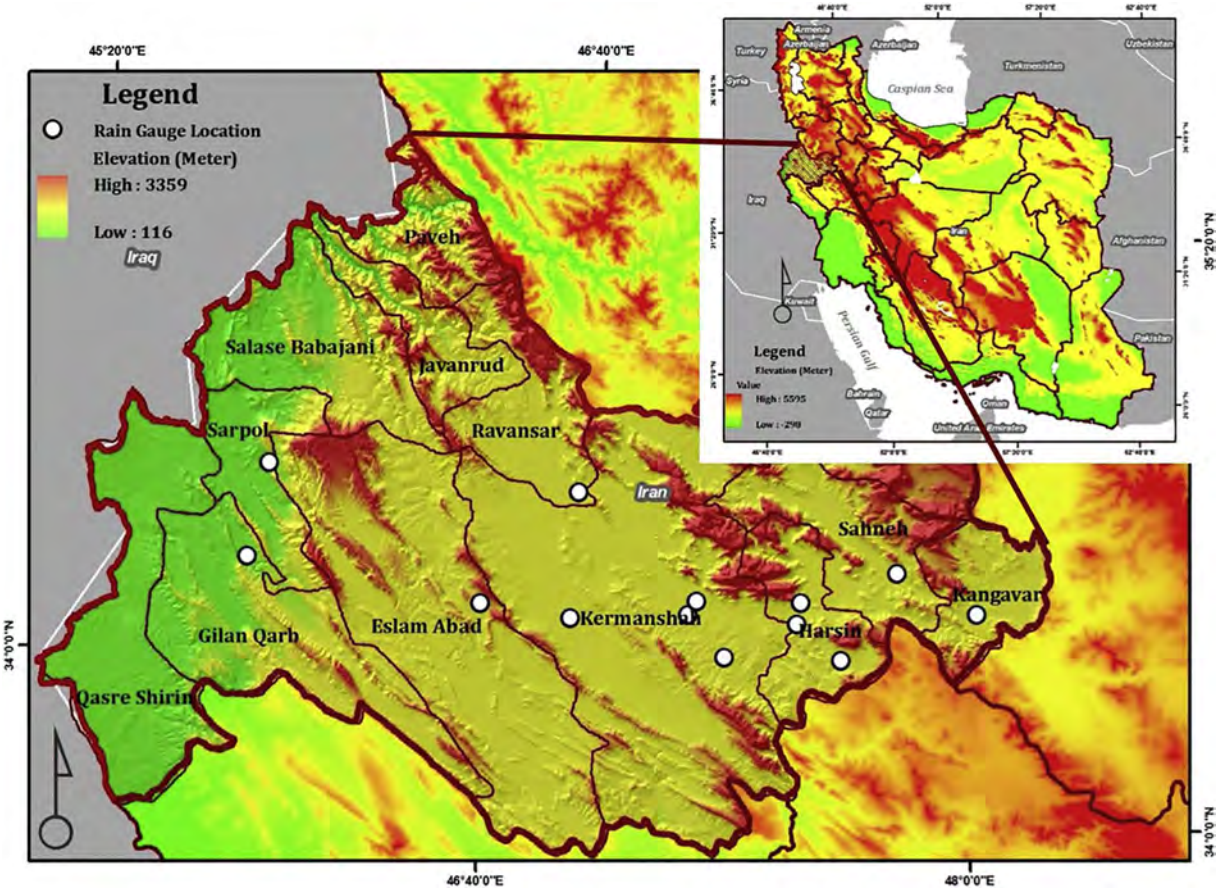

Fig. 1. Location map of the study area.

Moderate Resolution Imaging Spectroradiometers (MODIS). It is an 'optimised' index designed to enhance the vegetation signal with improved sensitivity in high biomass regions. It further improves vegetation monitoring through minimising both soil and atmosphere influences (Jiang et al., 2008). EVI is one of widely used satellite vegetation greenness indices which have been successfully used to monitor global vegetation photosynthetic activity (Huete et al., 2002; Jiang et al., 2008; Justice et al., 2002; Tucker, 1979). Drought indices derived from satellite imagery have been widely used to identify spatial extents of drought (Vergni and Todisco, 2011). The indices are useful for detection and monitoring large area vegetation stress resulted from drought or soil oversaturation following flooding and excessive rains. This soil and atmosphere resistant vegetation index is defined by (Solano et al., 2010):

$$EVI = \mathrm{G}\left(\frac{P_{nir} - P_{red}}{L + P_{nir} - C_1 P_{red} - C_2 P_{blue}}\right) \quad (1)$$

where P is 'apparent' (top-of-the-atmosphere) or 'surface' directional reflectance, L is a canopy background adjustment term equal to 1, G gain factor and another constant equal to 0.2 and C_1 and C_2 weigh the use of the blue channel in aerosol correction of the red channel estimated about 6 and 7.5, respectively.

3.3. One-class support vector machine

Support vector machine (SVM) is a supervised learning method derived from statistical learning theory and the structural risk minimization principle (Boser et al., 1992; Vapnik, 2013; Vapnik and Vapnik, 1998). It uses a decision surface to separates the target classes through maximisation of the margin between them (Burges, 1998). The mentioned surface is usually called the optimal hyperplane, and the data points closest to the hyperplane are called support vectors (Fig. 3). It should be noted that the support vectors are considered critical elements of the training set.

However, often support vector machines are an example of a linear two-class algorithms are aimed to maximize the margin between the two classes (Fig. 4a), it could be used for one-class classification purpose, where one tries to detect one class and reject the others (Fig. 4b) (Deo et al., 2017; Gunn, 1998; Muñoz-Marí et al., 2010).

The one-class support vector machine (OC-SVM) was proposed by (Schölkopf et al., 2001) to estimate a set that encloses most of a given random sample where $x_i \in R^d$. Each x_i is first transformed via a map $\varphi: R^d \to H$ where H is a high (possibly infinite) dimensional Hilbert space generated by a positive-definite kernel $k(x_i, y_i)$. The kernel function corresponds to an inner product in H through $k(x_i, y_i) = \langle \varphi(x_i), \varphi(y_i) \rangle$.The OC-SVM speculates a hyperplane in the feature space which detaches the data from the origin with maximum possible margin (Fig. 4b). In the event that no such hyperplane exists, slack variables ξ_i allow for some points to be within the margin, and the free parameter $v \in [0, 1]$ controls the cost of such violations. In fact, v can be shown to be an upper bound on the fraction of points within the margin (outliers) (Schölkopf et al., 2001). The hyperplane in feature space induces a generally nonlinear surface in the input space. More precisely, the OC-SVM as presented in (Schölkopf et al., 2001) (Tax and Duin, 1999) requires the solution of the following optimisation problem:

$$\min_{w,\, \xi,\, b} \left\{ \frac{1}{2} \| w \|^2 + \frac{1}{vl} \sum_{i=1}^{1} \xi_i - p \right\} \quad (2)$$

$$Subject - to \quad (w, \Phi(x_i)) \geq p - \xi_i, \quad \xi_i \geq 0. \quad (3)$$

Here, ω is a vector perpendicular to the hyperplane in H, and ρ is the

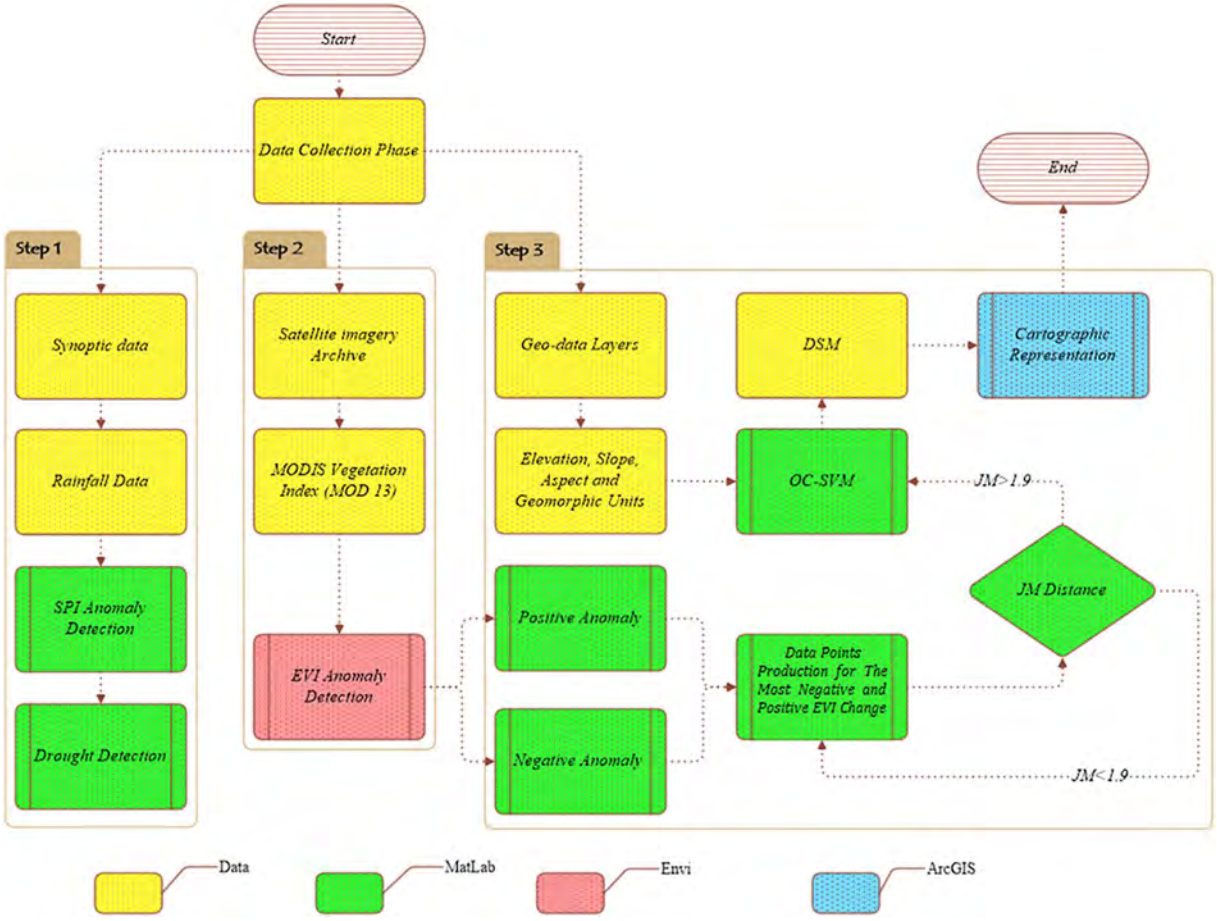

Fig. 2. Schematic representation of the 3-step methodology implementation.

Table 1
Drought category of SPI value (McKee et al., 1993).

SPI value	Drought category	Time in category (%)
0 to − 0.99	Mild	34.1
− 1.00 to − 1.49	Moderate	9.2
− 1.50 to − 1.99	Severe	4.4
≤ − 2.00	Extreme	2.3

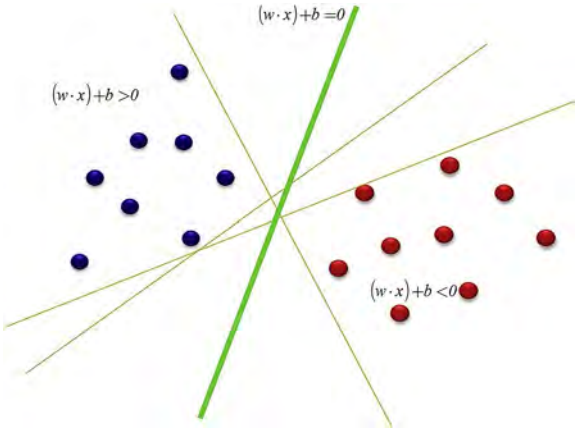

Fig. 3. Optimal separating hyperplane (Gunn, 1998).

distance to the origin. Since the training data distribution may contain outliers, a set of slack variables $\xi_i \geq 0$ is introduced to deal with them (which allows for penalised constraint violation), as usual in the SVM framework. The parameter $v \in [0,1]$ controls the trade-off between the number of examples of the training set mapped as positive by the decision function $f(x) = sng(w, \Phi(x_i)) - p$ and having a small value of $\|w\|$ to control model complexity. Finally, it must be noted that it is possible to segregate two patterns either through one two-class support vector machine (TC-SVM) or two OC-SVMs, which the latter produces more conservative decision regions (Elshinawy et al., 2010).

3.4. Kernel functions

The performance of the SVM model depends on the choice of the kernel parameters. Accordingly, selection of the kernel function is very important in SVM modelling (Xu et al., 2012). However new kernels are being proposed by researchers, four kinds of them are often used: linear kernel, polynomial kernel, RBF kernel (often called Gaussian kernel) and sigmoid kernel as the last one (Brereton and Lloyd, 2010; Hsu et al., 2003). In the present study, we have chosen RBF kernel as the most popular kernel functions of the SVM algorithm.

3.4.1. Radial basis functions (RBF)

RBF has received significant attention in various kernelized learning algorithms (Hsu et al., 2003). It is simply defined as:

$$k(x_i, x_j) = \exp(-\gamma \parallel x_i, x_j \parallel^2),\ \gamma > 0 \quad (4)$$

where $\gamma > 0$ is a parameter that controls the width of Gaussian distribution. It plays a similar role as the degree of the polynomial kernel in controlling the flexibility of the resulting algorithm (Ben-Hur and Weston, 2010).

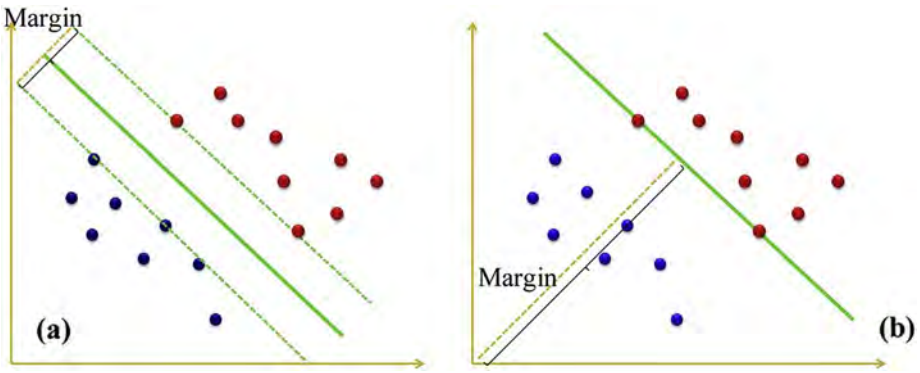

Fig. 4. Typical support vector machines classifiers: a) Two Class SVM (Gunn, 1998) b) One Class SVM (Muñoz-Marí et al., 2010).

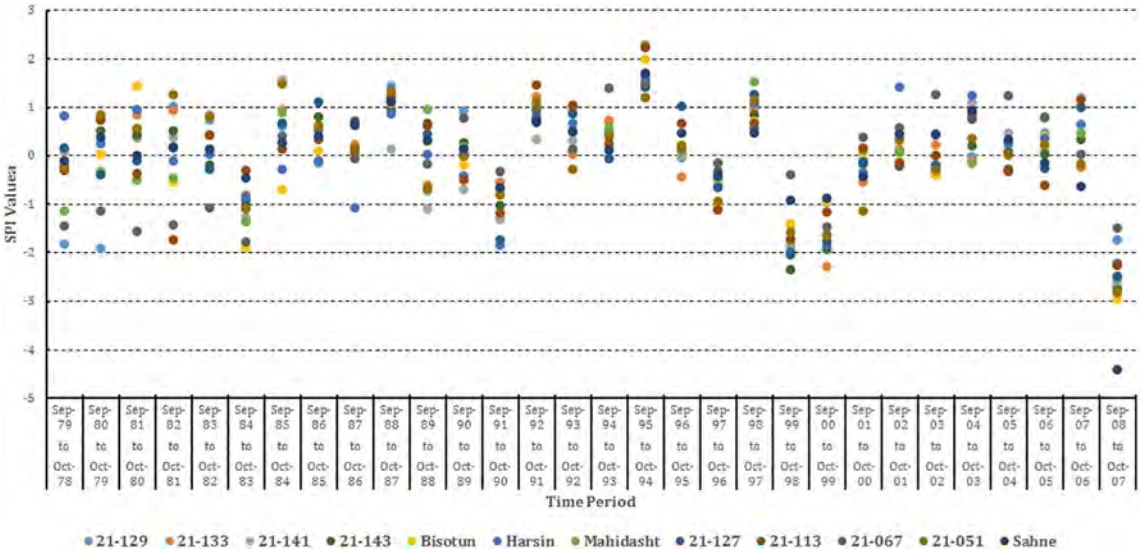

Fig. 5. Standardised precipitation index (SPI) for October 1978 through September 2008 with a time scale of 1 months.

3.5. Jeffries-Matusita (JM) separability measure

With respect to the fact that drought sensitivity mapping was the goal of the present study, the assessment focused on distinguishing the most sensitive from the least sensitive class. Here, separability degree of sensitivity classes was assessed through Jeffries-Matusita (JM) separability approach that used both training subsets including more and less sensitive location. The JM distance between a pair of class-specific probability functions is defined as following (Richards and Jia, 1999):

$$J_{ij} = \int_x \left(\sqrt{p(x \mid w_i)} - \sqrt{p(x \mid w_j)}\right)^2 dx \tag{5}$$

where $p(x|w_i)$ and $p(x|w_j)$ are conditional probability density functions for the feature vector x, given in data classes of w_i = more sensitive and w_j = less sensitive events respectively. Under normally distributed classes this becomes:

$$J_{ij} = 2(1 - e^{-B}) \tag{6}$$

where

$$B = \frac{1}{8}(m_i - m_j)^t \left\{\frac{\Sigma_i + \Sigma_j}{2}\right\}^{-1} (m_i - m_j) + \frac{1}{2} In \left\{\frac{\left|\left(\Sigma_i + \Sigma_j\right)/2\right|}{|\Sigma_i|^{\frac{1}{2}} + |\Sigma_j|^{\frac{1}{2}}}\right\} \tag{7}$$

In this notation, m_i and m_j correspond to class-specific, expected sensitivity values, and Σ_i and Σ_j are unbiased estimates for the class-specific covariance matrices of more and less sensitive subsets respectively, ln is the natural logarithm function, $|\Sigma_i|$ and $|\Sigma_j|$ are the determinant of Σ_i and Σ_j (matrix algebra). JM separability measure takes on a maximum value of 2.0, and values above 1.9 indicate assuring separability (Richards and Jia, 1999). For lower separability values, it should be taken into consideration to improve the separability by editing the position of more sensitive points which are located in less sensitive areas, vice versa. Here, the achieve value for the more and less sensitive separability measure was equal to 1.976 which suggests that the two more and less sensitive training subsets may be distinct with high separability.

4. Results

When drought occurs through an extended period, a region receives a deficiency in its water supply, whether atmospheric, surface or ground water. In other words, as a result of drought stream and river flows decline, water levels in lakes and reservoirs fall, and the depth to water in wells increases. This will further leads to decrease in soil moisture, which in long-term primary controls vegetation and ecosystems. Unlike the above mentioned immediate impacts of drought, however, long-term impacts could be harder to monitor and more costly to manage in the future. Here, we have used 30-years of monthly precipitation data for SPI calculation which was used to quantify the precipitation deficits for multiple time scales.

In this study, the SPI has been calculated for time-scales of 1 month for each year. Fig. 5 shows the SPI values for a time-scale of 1978 through 2008. As can been seen from Fig. 5, the minimum SPI value

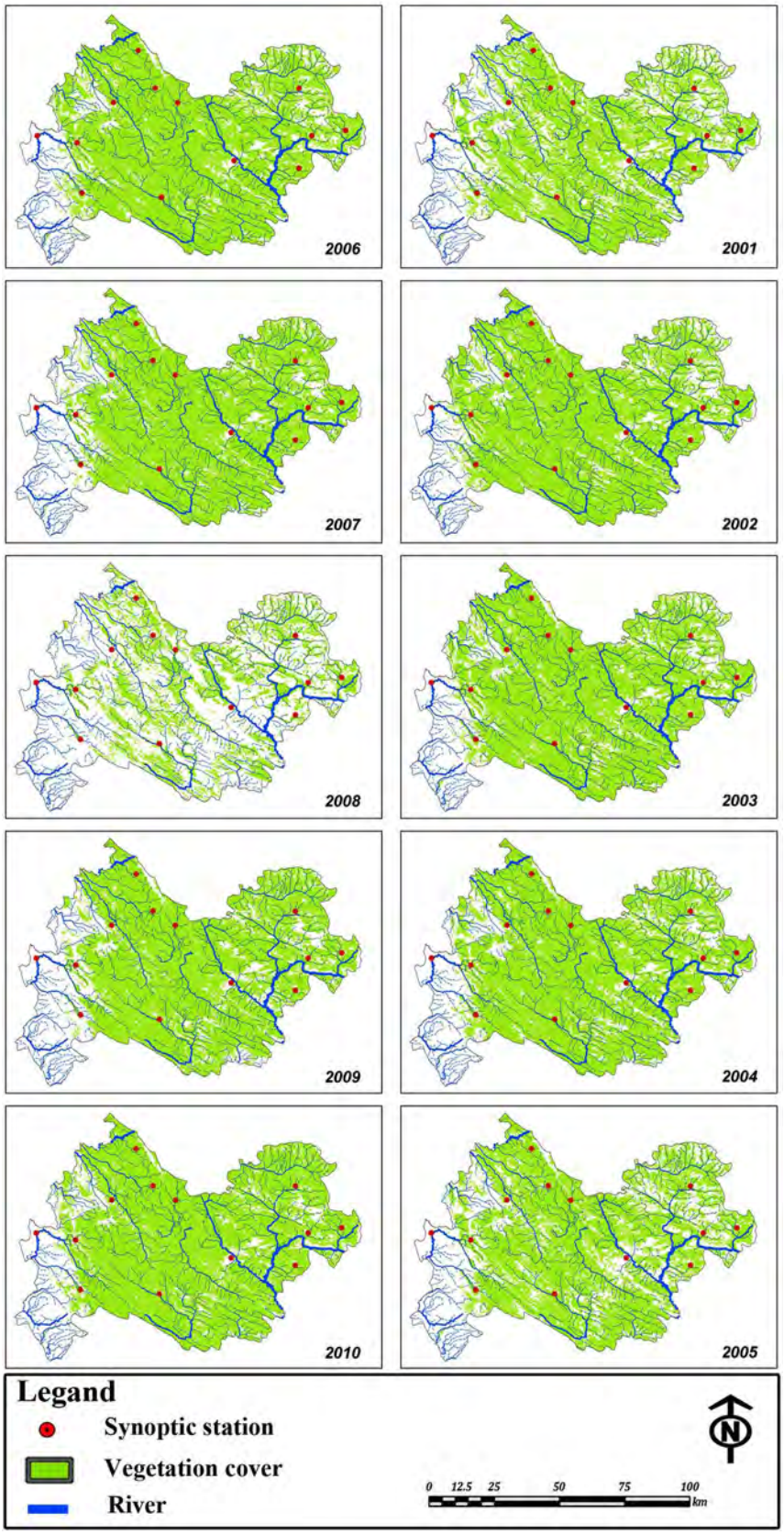

Fig. 6. Annual EVI values of late-April from 2001 to 2010.

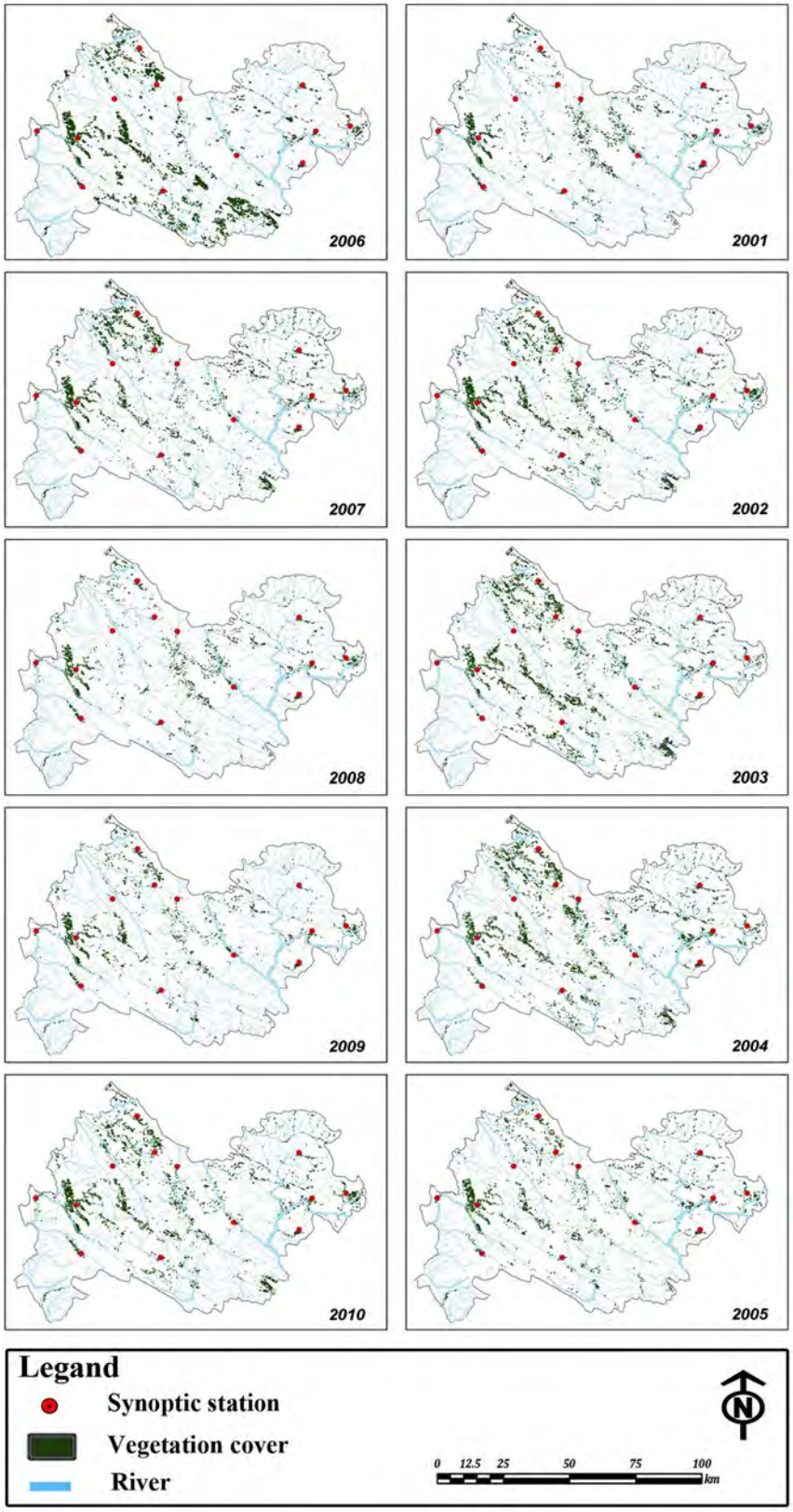

Fig. 7. Annual EVI values of mid-October from 2001 to 2010.

indicates a severe drought occurred in 2008 while the maximum SPI value belongs to 1995. Afterwards, we have also examined the spatio-temporal patterns of EVI values of late-April (the most monthly EVI value) and mid-October (the least monthly EVI value) through the entire study region from 2001 to 2010. Results of both SPI and EVI testify a severe drought occurrence in 2008 which was selected as the basis of DSM (Fig. 6).

In other words, considering the fact that there is no satellite imagery archive belonging to 1995 (i.e. maximum SPI value), we tried to use a pixel based ratio of average and minimum EVI values (i.e. 2006 and

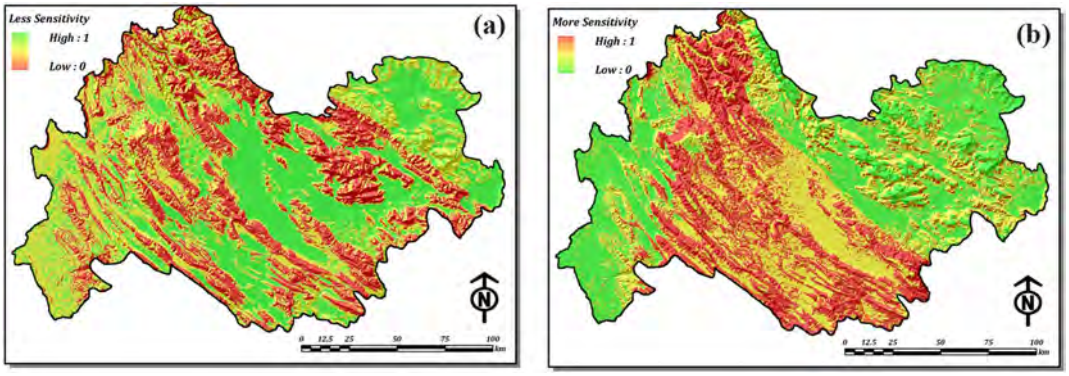

Fig. 8. Resultant outcome of each OC-SVM including: (a) more, and (b) less sensitive classes of proposed DSM scheme.

2008) for further identification of the least and the most vegetation loss locations. As EVI is found to be linearly correlated with green leaf area index (LAI) in crop fields (Jiang et al., 2008), it will be maximized when it is representing highest leaf biomass. Therefore, here in the present study, pixels with most positive changes in EVI value, representing an increase in the biomass amount of the pixel, were detected as the less sensitive pixels to drought. However, pixels with the most negative changes were considered as more sensitive (Fig. 7). In other words, considering the fact that leaf biomass will be reduced as results of drought impacts, the word 'less sensitive' has been chosen when leaf biomass is not negatively affected by drought. Nonetheless, the word 'more sensitive' is selected for the opposite condition.

The proposed model of DSM is based on the OC-SVM classification technique that could be considered as a quantitative soft computing method within which less subjectivity is guaranteed. In this respect, following the accomplishments of necessary data pre-processing steps, each criterion of the study area was divided into a 278 m ∗ 278 m square grid, which contains 320,563 pixels, laid out in an irregular boundary. Accordingly, after importing the pre-processed data into the MatLab environment, an evaluation matrix is then constructed to be used in the classification process. Experimental results not only showed that OC-SVM is more efficient compared to TC-SVM algorithm while producing results of similar accuracy, but also it requires less time and storage space to run compared to TC-SVM (Manevitz and Yousef, 2002; Senf et al., 2006). As a result, two OC-SVMs were applied by an RBF kernel function to construct the respective DSM in a further step (Fig. 8).

Finally, in the present study, the proposed DSM is divided into five sensitivity classes namely very low, low, moderate, high and very high using 2D scatter plots and nine fuzzy if-then rules (Fig. 9).

Fig. 9 illustrates how fuzzy if-then rules have been used for pattern classification problems while Fig. 10 represents final DSM of Kermanshah Province which has been elaborated using OC-SVM algorithms and

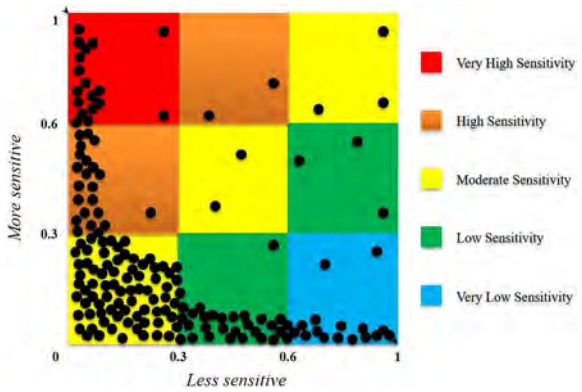

Fig. 9. Selected if-then rules for 2D scatter plots to interactively classify two categories of more and less sensitive pixels.

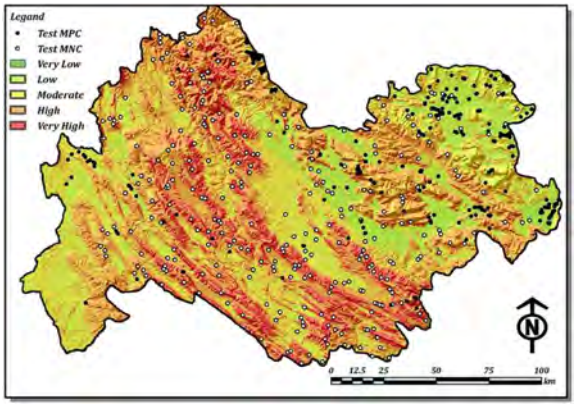

Fig. 10. Resultant sensitivity map of proposed DSM scheme along with the most negative and the most positive changes test data points of EVI.

corresponding geo-data layers including EVI, elevation, slope, aspect and geomorphic units.

4.1. Validation of the results

Validation is truly an essential step in the development of any predictive model and estimation of its reliability measure. The prediction efficiency of any geospatial predictive model and its resultant output (i.e. proposed DSM) is usually estimated by using independent information posterior to map elaboration. Therefore, here where we have used a separate training set, the accuracy of the proposed DSM technique in Kermanshah Province was evaluated by calculating relative operating characteristics (ROC) which depict the capability of a binary algorithm system as its discrimination threshold changes (Fawcett, 2006; Feizizadeh et al., 2014; Sabokbar et al., 2014). We have also used a simple overlay technique to show the percentage of known changes of EVI in various sensitivity classes.

Considering the ROC method, the area under the ROC curve (AUC) values, varying between 0.5 and 1.0, is used to evaluate the accuracy of the DSM. The AUC defines the accuracy of the proposed probabilistic model through describing the model ability to reliably predict the occurrence or non-occurrence of an event. The ideal model shows an AUC value close to 1.0, whereas a value close to 0.5 indicates inaccuracy in the model (Fawcett, 2006; Roodposhti et al., 2014; Shahabi and Hashim, 2015). In order to apply the ROC method, a concise and representative dataset was prepared using randomly selected 278 first negative along with 278 first positive points of EVI change throughout the study area. As it is assumed that changing EVI values are representative of drought impacts on vegetation cover, these points will be further used to evaluate the accuracy of sensitivity maps proposed by two OC-SVM algorithms. The AUC value of ROC curve for the output map was found to be 0.809, with an estimated standard error

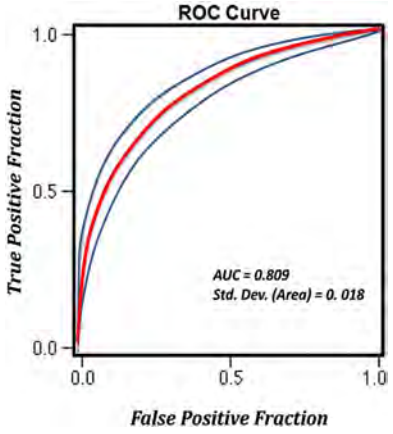

Fig. 11. ROC curve for the proposed DSM using two OC-SVM class.

of 0.01 (Fig. 11).

The DSM results were also verified using the test inventory data points itself. Accordingly, these 278 first negative along with 278 first positive points of EVI change locations were overlaid on the proposed DSM map (Fig. 12). The result shows that 197 data points which represent vegetation lost (70.86% of all test data for negative changes) overlaid on the high and very high sensitive patches, which they only cover 14,657 km^2 (59.1%) of the study area while only 1 test data appears in the very low sensitive zone.

In addition to the above, it should be mentioned that about 185 (66.5% of all test data for positive changes of EVI value) data points which represent positive change in EVI value overlaid on the low and very low sensitivity zones, which they only cover 3963 km^2 (15.9%) of the study region while only 10 test data appears in the very high sensitive class.

5. Short discussion and conclusions

Considering the most important factors which cause the present conditions of sensitivity to drought being in place in the study region, there was a demand to conduct a reliable DSM for vegetation cover. The reliability of DSM depends not only on the presence of concise and representative database, in terms of data scale and accuracy, but also on the selection of the appropriate DIs for and drought identification and severity evaluation. Regardless of data scale and accuracy, the present study aimed to explore DSM of Kermanshah by using both climatic and satellite-based DI which were used to confirm mild and severe drought occurrence and resultant vegetation loss. Further, an objective classification scheme along with four different drought-related geo-data layers were used in order to produce a reliable DSM.

Results of the analysis showed notable spatio-temporal variation in terms of vegetation sensitivity to drought phenomena throughout the study area. In this respect, the elevation class of 1500 to 2000 m, slope classes between 4 and 32 degree, aspect classes of south and south-west (May) or east and north-east (October) and Zagros Orogenic Belt are the most affected from drought periods. However, slope classes between 2 and 4 degree (both in May and October) or more that 32 degrees (October), elevation less than 1500 m (both in May and October) or more than 2500 m (October) and Sanandaj-Sirjan geomorphic zone are the least affected by drought periods.

According to the obtained results, the resistance of vegetation to drought occurrence may be mediated through the effects of topography (elevation, slope and aspect) on soils and microclimate. In this respect, the obtained results of proposed DSM testify that plants in higher elevations (i.e. above 1500 m to 2500 m) typically are more affected by drought, compared with the similar plants of lower elevation (below 1500 m). This is mainly correspondent to the negative correlation between slope gradient and soil moisture which is statistically more significant in higher elevations where steep slopes prevail. On the other hands, depth of soil horizons is significantly increased by a decrease in elevation. Accordingly, soils at lower elevations of the slope (i.e. Cambiosol and Litosol) may have larger sources of water compared to the soils in higher elevation. Natural vegetation cover is relatively drought-tolerant at elevations above 2500 m because of consistent snow coverage which increases soil moisture and decreases environmental temperature.

Consequently, the spatial variation in soil moisture is also controlled by slope angle and aspect. Here, drought impacts on vegetation loss more obvious within southern and eastern slope and the slope angle more than 8 degrees while it is less obvious in northern and western slope and the slope angle between the 0–4. The magnitude soil moisture was found to decrease not only with an increase in angle of slope and but also with a topographic solar radiation index derived from slope angle and slope aspect.

Considering geomorphic units criterion, it has been found that Sanandaj-Sirjan unit is less sensitive to the occurred drought events compared to different parts of Zagros Orogenic Belt (i.e. Zagros Thrust or Folded Zagros zone). This is mainly related to some primary variables such as the surface materials and elevation which further affects other secondary variables including temperature, evapotranspiration and snow accumulation coefficient.

As a matter of fact, this study not only presents an integrated strategic DSM framework with an emphasis on solving the decision problem by using an objective procedure. In other words, this article introduces the use of the enhanced vegetation index (EVI) as an indicator of soil moisture while it focuses on producing a drought sensitivity map (DSM) for vegetation cover using two one-class support vector machine algorithms. Finally, considering the fact that, the

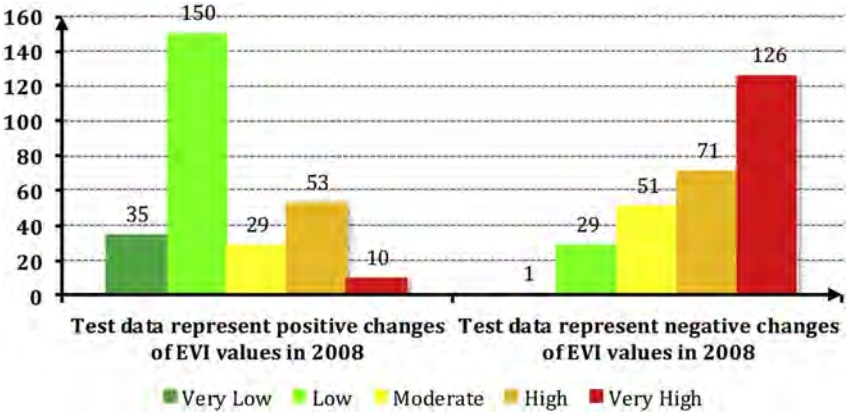

Fig. 12. Histogram of test data overlay showing the relative areas for each sensitivity class (each class is labeled with the number of the observed negative or positive test data accordingly).

proposed schematic framework has the advantage of satellite imagery archive as ground truth; it can be used for production DSM of different local or regional scales. On the other hand, the proposed DSM scheme can be further extended by using more drought-related criteria including vegetation type, soil depth, drainage density etc. through different case studies.

Acknowledgment

The authors would like to thank for anonymous reviewers and editor for their valuable and constructive comments on the earlier version of the manuscript.

References

Aydin, M., 1995. Water key ingredient in Turkish farming. In: Forum for Applied Research and Public Policy, .
Bannayan, M., Sanjani, S., Alizadeh, A., Lotfabadi, S.S., Mohamadian, A., 2010. Association between climate indices, aridity index, and rainfed crop yield in northeast of Iran. Field Crop Res. 118, 105–114.
Belal, A.-A., El-Ramady, H.R., Mohamed, E.S., Saleh, A.M., 2014. Drought risk assessment using remote sensing and GIS techniques. Arab. J. Geosci. 7, 35–53.
Ben-Hur, A., Weston, J., 2010. A user's guide to support vector machines. In: Data Mining Techniques for the Life Sciences, pp. 223–239.
Bhuiyan, C., Singh, R., Kogan, F., 2006. Monitoring drought dynamics in the Aravalli region (India) using different indices based on ground and remote sensing data. Int. J. Appl. Earth Obs. Geoinf. 8, 289–302.
Bird, D.K., 2009. The use of questionnaires for acquiring information on public perception of natural hazards and risk mitigation–a review of current knowledge and practice. Nat. Hazards Earth Syst. Sci. 9, 1307–1325.
Boser, B.E., Guyon, I.M., Vapnik, V.N., 1992. A training algorithm for optimal margin classifiers. In: Proceedings of the Fifth Annual Workshop on Computational Learning Theory, ACM, pp. 144–152.
Brereton, R.G., Lloyd, G.R., 2010. Support vector machines for classification and regression. Analyst 135, 230–267.
Burges, C.J., 1998. A tutorial on support vector machines for pattern recognition. Data Min. Knowl. Disc. 2, 121–167.
Burton, I., 1993. The Environment as Hazard. Guilford Press.
Cancelliere, A., Di Mauro, G., Bonaccorso, B., Rossi, G., 2007. Drought forecasting using the standardized precipitation index. Water Resour. Manag. 21, 801–819.
Chang, N.-B., Yang, Y.J., Goodrich, J.A., Daranpob, A., 2010. Development of the metropolitan water availability index (MWAI) and short-term assessment with multi-scale remote sensing technologies. J. Environ. Manag. 91, 1397–1413.
Cui, Q.-L., Wu, H.-N., Shen, S.-L., Xu, Y.-S., Ye, G.-L., 2015. Chinese karst geology and measures to prevent geohazards during shield tunnelling in karst region with caves. Nat. Hazards 77, 129–152.
Dai, A., 2011. Characteristics and trends in various forms of the Palmer drought severity index during 1900–2008. J. Geophys. Res. Atmos. 116.
Dai, A., Trenberth, K.E., Qian, T., 2004. A global dataset of Palmer drought severity index for 1870–2002: relationship with soil moisture and effects of surface warming. J. Hydrometeorol. 5, 1117–1130.
Deo, R.C., Kisi, O., Singh, V.P., 2017. Drought forecasting in eastern Australia using multivariate adaptive regression spline, least square support vector machine and M5Tree model. Atmos. Res. 184, 149–175.
Elshinawy, M.Y., Badawy, A.-H.A., Abdelmageed, W.W., Chouikha, M., 2010. Comparing one-class and two-class SVM classifiers for normal mammogram detection. In: Applied Imagery Pattern Recognition Workshop (AIPR), 2010 IEEE 39th, IEEE, pp. 1–7.
Fawcett, T., 2006. An introduction to ROC analysis. Pattern Recogn. Lett. 27, 861–874.
Feizizadeh, B., Roodposhti, M.S., Jankowski, P., Blaschke, T., 2014. A GIS-based extended fuzzy multi-criteria evaluation for landslide susceptibility mapping. Comput. Geosci. 73, 208–221.
Gunn, S.R., 1998. Support vector machines for classification and regression. In: ISIS Technical Report. 14.
Hayes, M., Svoboda, M., Wall, N., Widhalm, M., 2011. The Lincoln declaration on drought indices: universal meteorological drought index recommended. Bull. Am. Meteorol. Soc. 92, 485–488.
He, Y., Ye, J., Yang, X., 2015. Analysis of the spatio-temporal patterns of dry and wet conditions in the Huai River Basin using the standardized precipitation index. Atmos. Res. 166, 120–128.
Houghton, J., et al., 2001. Climate Change 2001: The Scientific Basis. Cambridge University Press, Cambridge.
Hsu, C.-W., Chang, C.-C., Lin, C.-J., 2003. A Practical Guide to Support Vector Classification .
Huete, A., et al., 2002. Overview of the radiometric and biophysical performance of the MODIS vegetation indices. Remote Sens. Environ. 83, 195–213.
Jain, S.K., Keshri, R., Goswami, A., Sarkar, A., 2010. Application of meteorological and vegetation indices for evaluation of drought impact: a case study for Rajasthan, India. Nat. Hazards 54, 643–656.
Jairath, J., 2008. Droughts and Integrated Water Resource Management in South Asia: Issues, Alternatives and Futures. SAGE Publications.
Jiang, Z., Huete, A.R., Didan, K., Miura, T., 2008. Development of a two-band enhanced vegetation index without a blue band. Remote Sens. Environ. 112, 3833–3845.
Justice, C., et al., 2002. An overview of MODIS Land data processing and product status. Remote Sens. Environ. 83, 3–15.
Karavitis, C.A., Alexandris, S., Tsesmelis, D.E., Athanasopoulos, G., 2011. Application of the standardized precipitation index (SPI) in Greece. Water 3, 787–805.
Keyantash, J., Dracup, J.A., 2002. The quantification of drought: an evaluation of drought indices. Bull. Am. Meteorol. Soc. 83, 1167.
Li, J., Chen, F., Cook, E.R., Gou, X., Zhang, Y., 2007. Drought reconstruction for north central China from tree rings: the value of the Palmer drought severity index. Int. J. Climatol. 27, 903–909.
Lioubimtseva, E., Adams, J., 2004. Possible implications of increased carbon dioxide levels and climate change for desert ecosystems. Environ. Manag. 33, S388–S404.
Liu, X., et al., 2013. Dynamic risk assessment of drought disaster for maize based on integrating multi-sources data in the region of the northwest of Liaoning Province, China. Nat. Hazards 65, 1393–1409.
Manevitz, L.M., Yousef, M., 2002. One-class SVMs for document classification. J. Mach. Learn. Res. 2, 139–154.
McKee, T.B., Doesken, N.J., Kleist, J., 1993. The relationship of drought frequency and duration to time scales. In: Proceedings of the 8th Conference on Applied Climatology. American Meteorological Society Boston, MA, USA, pp. 179–183.
Mu, Q., Zhao, M., Kimball, J.S., McDowell, N.G., Running, S.W., 2013. A remotely sensed global terrestrial drought severity index. Bull. Am. Meteorol. Soc. 94, 83–98.
Muñoz-Marí, J., Bovolo, F., Gómez-Chova, L., Bruzzone, L., Camp-Valls, G., 2010. Semisupervised one-class support vector machines for classification of remote sensing data. IEEE Trans. Geosci. Remote Sens. 48, 3188–3197.
Narasimhan, B., Srinivasan, R., 2005. Development and evaluation of soil moisture deficit index (SMDI) and evapotranspiration deficit index (ETDI) for agricultural drought monitoring. Agric. For. Meteorol. 133, 69–88.
Pai, D., Sridhar, L., Guhathakurta, P., Hatwar, H., 2011. District-wide drought climatology of the southwest monsoon season over India based on standardized precipitation index (SPI). Nat. Hazards 59, 1797–1813.
Quesney, A., et al., 2000. Estimation of watershed soil moisture index from ERS/SAR data. Remote Sens. Environ. 72, 290–303.
Richards, J., Jia, X., 1999. Remote Sensing Digital Image Analysis. Springer, New York.
Roodposhti, M.S., Rahimi, S., Beglou, M.J., 2014. PROMETHEE II and fuzzy AHP: an enhanced GIS-based landslide susceptibility mapping. Nat. Hazards 73, 77–95.
Sabokbar, H.F., Roodposhti, M.S., Tazik, E., 2014. Landslide susceptibility mapping using geographically-weighted principal component analysis. Geomorphology 226, 15–24.
Schölkopf, B., Platt, J.C., Shawe-Taylor, J., Smola, A.J., Williamson, R.C., 2001. Estimating the support of a high-dimensional distribution. Neural Comput. 13, 1443–1471.
Seddon, A.W., Macias-Fauria, M., Long, P.R., Benz, D., Willis, K.J., 2016. Sensitivity of global terrestrial ecosystems to climate variability. Nature 531, 229–232.
Senf, A., Chen, X.-W., Zhang, A., 2006. Comparison of one-class SVM and two-class SVM for fold recognition. In: Neural Information Processing. Springer, pp. 140–149.
Shafer, B., Dezman, L., 1982. Development of a surface water supply index (SWSI) to assess the severity of drought conditions in snowpack runoff areas. In: Proceedings of the Western Snow Conference. Colorado State University Fort Collins, CO, pp. 164–175.
Shahabi, H., Hashim, M., 2015. Landslide susceptibility mapping using GIS-based statistical models and Remote sensing data in tropical environment. Sci. Rep. 5.
Solano, R., Didan, K., Jacobson, A., Huete, A., 2010. MODIS vegetation index user's guide (MOD13 series). In: Vegetation Index and Phenology Lab, .
Son, N., Chen, C., Chen, C., Chang, L., Minh, V., 2012. Monitoring agricultural drought in the Lower Mekong Basin using MODIS NDVI and land surface temperature data. Int. J. Appl. Earth Obs. Geoinf. 18, 417–427.
Sönmez, F.K., KÖmÜscÜ, A.Ü., Erkan, A., Turgu, E., 2005. An analysis of spatial and temporal dimension of drought vulnerability in Turkey using the standardized precipitation index. Nat. Hazards 35, 243–264.
Tax, D.M., Duin, R.P., 1999. Support vector domain description. Pattern Recogn. Lett. 20, 1191–1199.
Toulios, L., et al., 2012. Capitolo III potential of remote sensing to support the assessment of climate change and variability on European agriculture. In: Climate Change Impacts on Agriculture in Europe, pp. 93.
Tucker, C.J., 1979. Red and photographic infrared linear combinations for monitoring vegetation. Remote Sens. Environ. 8, 127–150.
Vapnik, V., 2013. The Nature of Statistical Learning Theory. Springer Science & Business Media.
Vapnik, V.N., Vapnik, V., 1998. Statistical Learning Theory. Wiley, New York.
Vergni, L., Todisco, F., 2011. Spatio-temporal variability of precipitation, temperature and agricultural drought indices in Central Italy. Agric. For. Meteorol. 151, 301–313.
Vicente-Serrano, S.M., et al., 2012. Performance of drought indices for ecological, agricultural, and hydrological applications. Earth Interact. 16, 1–27.
Werick, W., Willeke, G., Guttman, N., Hosking, J., Wallis, J., 1994. National drought atlas developed. EOS Trans. Am. Geophys. Union 75, 89–90.
Wilhite, D.A., 2012. Drought Assessment, Management, and Planning: Theory and Case Studies: Theory and Case Studies. Springer Science & Business Media.
Xu, C., Dai, F., Xu, X., Lee, Y.H., 2012. GIS-based support vector machine modeling of earthquake-triggered landslide susceptibility in the Jianjiang River watershed, China. Geomorphology 145, 70–80.
Zambrano, F., Wardlow, B., Tadesse, T., Lillo-Saavedra, M., Lagos, O., 2017. Evaluating satellite-derived long-term historical precipitation datasets for drought monitoring in Chile. Atmos. Res. 186, 26–42.
Zhang, Q., Xu, C.-Y., Zhang, Z., 2009. Observed changes of drought/wetness episodes in the Pearl River basin, China, using the standardized precipitation index and aridity index. Theor. Appl. Climatol. 98, 89–99.